Nanoplastics induce more severe apoptosis through mitochondrial damage in Caco-2 cells compared to sub-micron plastics

Zifan Lu
Guangdong Ocean University
Yuanyuan Zhang
Shenzhen Institute of Guangdong Ocean University
Lei He
Guangdong Ocean University
Chunxia Zhou
Guangdong Ocean University
Pengzhi Hong
Guangdong Ocean University
Zhong-Ji Qian
Guangdong Ocean University
Xianghong Ju
Guangdong Ocean University
Shengli Sun
Guangdong Ocean University
Chengyong Li (cyli@gdou.edu.cn)
Guangdong Ocean University

Research Article

Keywords: Microplastics, Caco-2 cell, Mitochondria, Apoptosis, Methylmercury

Posted Date: March 10th, 2022

DOI: https://doi.org/10.21203/rs.3.rs-1417473/v1

Abstract

Background

Small plastic particles such sub-micron- (1μm-100nm) and nanoplastics (<100nm) derived from the environment can enter the human gastrointestinal tract through the food chain. In addition, MPs adsorbed with heavy metals are synergistically toxic to humans. Though the cytotoxicity of different sizes of polystyrene (PS) has been studied, the toxicity study of small sizes PS such as 20 nm on intestinal cells is still utterly limited.

Results

In the present study, the toxicity of 20 nm and 200 nm PS (PS20, PS200) on Caco-2 cells was investigated. PS20 could disrupt cell membrane integrity at a concentration of 80 μg/mL. The images of laser scanning-confocal illustrated that cell tend to uptake more PS20 than PS200 and those particles were localized in lysosomes and mitochondria. Moreover, the loss of mitochondrial membrane potential of PS20 was more severe than that of PS200, which may account for the significant increase in reactive oxygen species (ROS) levels in the PS20-treated group. Furthermore, PS20 induced cell apoptosis. Moreover, PS enhanced the cytotoxicity of Methylmercury (MeHg). Overall, this study demonstrates that PS had a size- and concentration-dependent cytotoxic effect on the intestine and an enhanced cytotoxic effect on MeHg.

Conclusions

Both sub-micron and NPs could enter Caco-2 cells. NPS induced apoptosis by inducing mitochondrial damage and was significantly more toxic to cells than sub-micron PS. Both sizes of PS used in the experiments have a synergistic effect on MeHg-induced cytotoxicity. In conclusion, our study demonstrated the strong cytotoxicity of NPs and synergistic toxicity with heavy metals, providing a reference for the environmental toxicity of nanoscale plastics.

Background

In the nanoscience research community definition of nanomaterials, microplastics (MPs) are usually defined as particles between 100 nm and 5 mm in size, and nanoplastics (NPs) are particles less than 100 nm in size [1]. MPs have become the word of the day in terms of pollution. They exist all over the planet, and traces of them can be found in sediments thousands of meters deep in the ocean [2]. MPs pollution had reached its latest height on Earth when MPs appeared at 8440 m on Mount Everest [3]. Global production and use of plastics will remain on the rise until alternatives to biodegradable materials are widely available [4](Jambeck, 2015 #46).

MPs have negative impact on numerous marine habitats and biota [5, 6]. Importantly, they have been regarded as a threat to food safety. It has been reported that different types and sizes of MPs exist in

foods such as mineral water [7], salt [8, 9], beer and honey [10]. And a large amount of MPs would be released when the food packaging are heated and then ingested by humans [11]. The status of MPs in the oceans has been studied but has always been underestimated [12]. MPs are often eaten by mistake by small commercial seafood and then transfer to human tables through the food chain [8, 13]. A study of farmed oysters off the coast of China found that MPs were detected in 86% of the oysters sampled, with an average level of 0.62 particles/g [14]. Additionly, the evidence of plastic debris transfer along food chains has been provided [15, 16]. Previous studies have pointed out the potential role of MPs and NPs as carriers of hydrophobic organic chemicals, antibiotics, pathogens and heavy metals [17, 18, 19, 20], which affect living organisms and food safety.

The airborne plastic particles can be inhaled by human [21], however, due to the hydrophobicity, inhaled MPs and NPs may be rejected by the lung wall through the mucociliary clearance system [22]. Therefore, only a small proportion of particles may reach the lungs [21]. Notably, the uptake of MPs involves the whole body only when they were absorbed through the intestinal barrier and distributed to organs and tissues through the lymphatic or blood system. *In vitro* studies have indicated that micro/nano plastic can cross the intestinal barrier [23]. It has been demonstrated that carboxyl-surfaced PS nanoparticles can attach to the surface of red blood cells due to van der Waals forces, electrostatic forces, hydrogen bonding forces and hydrophobic interactions, subsequently, and can penetrate into the cell interior [24, 25]. Those interaction forces prevent PS nanoparticles from eliminating by the liver and spleen timely, and thus promote the PS circulation in the body. For instance, Wick et al. [26] conducted a placental barrier permeability of 240 nm PS to placental barrier. Yang et al. [27] demonstrated the blood brain barrier permeability of 20 nm PS by implanting microdialysis probes injected with fluorescent PS nanoparticles into the cerebral cortex of rats. Generally, small-sized NPs have the potential to overcome the tissue barrier function and, finally, reach the organs of the body through blood transportation.

The toxicity of microplastic particle usually has a negative relationship with size [28, 29]. Brown et al. [28] found that 64 nm PS resulted in a significant increase of Ca^{2+} levels in monomac-6 cells compared to larger PS (202 nm and 525 nm). Similarly, in A549 cell, 25 nm PS induced higher cytotoxicity than 70 nm PS [30]. In recent years, researchers noted that the gastrointestinal tract is susceptible to MPs than other organs [22, 31]. However, current studies mainly focus on the effects of MPs (>50 nm) on intestinal epithelial cells [32, 33]. Therefore, it's necessary to investigate the effect of smaller size (<50 nm) and plain PS on intestinal cells.

In this study, 200 nm PS and 20 nm PS represent sub-micron plastics and nanoplastics, respectively. We measured cytotoxicity, intracellular ROS level, cell membrane integrity, mitochondrial membrane potential and DNA damage of Caco-2 cells after exposure to PS with 20 nm and 200 nm at various concentrations. In addition, the fate of PS was also assessed after ingestion by the cells. Furthermore, the combined toxicity of PS and MeHg on Caco-2 cells was assessed.

Materials And Methods

Characterization

Two types of PS20 and PS200 were purchased from Huge Biotechnology (Shanghai, China). One was green fluorescent PS (excitation/emission wavelengths: 470 nm/525 nm), which was used for the cell uptake experiments. The second was virgin PS, which was used for cytotoxicity assays. The size and zeta potential of virgin PS were measured by laser particle size analyzer (LS13320, Beckman). The average hydrodynamic diameter and zeta potential of PS were measured with diluted deionized water and culture medium at 25 ℃. Virgin and fluorescent PS morphology in water was measure by transmission electron microscope (JEM-1400, Japan).

Cell culture

Human colon adenocarcinoma Caco-2 cells were obtained from Cell Bank of Chinese Academy of Sciences (Shanghai, China), and grown in RPMI-1640 medium (Gibco, USA), which is supplemented with 10% fetal bovine serum (Vigonob, Uruguay) and 1% antibodies (100 U/mL penicillin/streptomycin) (Gibico, USA). Cell cultureed under standard conditions (37 ℃ and 5% CO2).

Cell viability

Viability of Caco-2 cells after 6 h of exposure to PS was measured using a cell counting kit-8 (Apexbio, USA). Caco-2 cells were seeded at a density of $1´10^5$ cells/well in 96-well plates. After PS exposure (20, 40, 60, 80 and 100 μg/mL), 10 μL of CCK-8 solution was added to each well of 96-well plate, following by incubation for 1 h. Absorbance of the mixture was measured at 450 nm using a microplate reader. The absorbance of the mixture at 600 nm was also measured to eliminate the PS light scattering. Cell viability was calculated based on the relative absorbance compared with the control group.

Glutathione (GSH) analysis

Cellular glutathione content was evaluated according to the manufacturer's instructions (Elabscience, Wuhan, China). Caco-2 cells were seeded at a density of $1´10^6$ cells/well in 6-well plate and the cells treated with PS20 and PS200. After 6 h, the cells were collected and subjected to lysis according to instructions. The supernatant was collected after centrifugation (1000×g, 4℃) and stored at -80℃ for further detection. The content of GSH was obtained by the calculation of total glutathione (T-GSH) and oxidized glutathione content. The absorbance was detected at 412 nm with a microplate reader.

Lactate dehydrogenase (LDH) analysis

Caco-2 cells were seeded at a density of $1´10^5$ cells/well in 96-well plate. After 6 h of exposure to PS, LDH assay was performed according to the manufacturer’s instructions (Beyotime, Shanghai, China). The absorbance of the supernatant at 490 nm was measured for each experimental group using a microplate reader. The LDH values were calculated by comparing the LDH activity of PS-treated cells with the maximum LDH activity control obtained after the addition of lysis buffer.

Intracellular ROS analysis

Intracelluar ROS indcued by PS exposure in Caco-2 cells were measured using Reactive oxygen species assay kit (Solarbio, Beijing, China). Hoechst 33342 (Beyotime, Shanghai) was used to normalize the number of cells in each well. In brief, the Caco-2 cells were seeded at a density of $1´10^5$ cells/well in 96-well plate. After 6 h of exposure of PS, 10 μM DCFH-DA and 2.5 μg/mL Hoechst 33342 were added to each well. After a 20-min incubation at 37 °C the cells were washed with PBS three times. A microplate reader (Thermo arioskan Flash, USA) was applied to measure the fluorescence values of DCF and Hoechst 33342. The excitation/emission wavelengths for DCF and Hoechst 33342 were 488/525 and 350/460 nm, respectively. The normalized DCF fluorescence values of the treated group were calculated compared with control group.

Intracellular quantification of PS

Caco-2 cells were seeded at a density of $2´10^5$ cells/well in 24-well plate and the cells treated with PS20 and PS200. After 6 h incubation with fluorescence PS, cells were washed with PBS thrice and lysed with 0.1 M NaOH solution. The lysed samples were transferred in black 96-well plate and readily detected by a fluorescent microplate reader (excitation: 470 nm, emission: 525 nm). The amount of intracellular fluorescent PS was calculated by substituting into the standard curve (Fig. S1).

Endocytosis of PS by Caco-2 cells

Caco-2 cells were seeded at a density of $1´10^6$ cells/dish in laser confocal cell culture dish (NEST, China) and cultured for 24 h. After 6 h of exposure to florescent PS, cells were fixed with 4% paraformaldehyde for 15 min and washed with 0.1% Triton X-100 (prepared by PBS, pH=7.4) thrice for Actin-red staining. The Actin-red solution (diluted at 1:50 with PBS containing 1% BSA and 0.1% Triton x-100) was added to the cells for 2 h at room temperature in the dark. Sequentially, cells were washed with PBS thrice, and were incubated with antifade mounting medium containing DAPI (Beyotime, China). The cells were observed by a laser confocal scanning electron microscope (FV3000, Olympus).

Lysosomal tracking of PS

Caco-2 cells were seeded at a density of $1´10^6$ cells/dish in laser confocal cell culture dish and cultured for 24 h. After exposure to florescent PS for 6 h, Caco-2 cells were washed with PBS three times. The LysoTracker-Red solution (50 nM) was added to the cells and incubated for 30 min. Finally, the cells were wash thrice with PBS containing 0.1% Triton x-100 and observed by a laser confocal scanning electron microscope (FV3000, Olympus).

Mitochondria tracking of PS

Caco-2 cells were seeded at a density of $1´10^6$ cells/dish in laser confocal cell culture dish and cultured for 24 h. After exposure to florescent PS for 6 h, the cells were incubated with MitoTracker-Red (100 nM)

for 30 min in the dark. The cells were wash thrice with PBS containing 0.1% Triton X-100 and observed by a laser confocal scanning electron microscope (FV3000, Olympus).

TEM (Transmission Electron Microscope) analysis

Caco-2 cells were seeded at a density of $1´10^6$ cells/well in 6-well plates and cultured for 24 h. After exposure to PS for 6 h, cells were harvested by centrifugation at 1000 rpm for 5 min. Cells were fixed with 3% glutaraldehyde for 2 h at 4°C and rinsed three times with 0.1 M PBS (pH 7.0) for 15 min each. After fixation with 1% osmium tetroxide for 1-2 h, the samples were rinsed three times with 0.1 M PBS (pH 7.0) for 15 min each. Samples were dehydrated with different concentrations of ethanol solutions (including five concentrations of 30%, 50%, 70%, 80%, 90% and 95%) for 15 min each, followed by treatment with 100% ethanol for 20 min. Samples were treated with pure acetone for 20 min, then with a mixture of encapsulant and acetone, and finally with pure encapsulant overnight. The permeation-treated samples were embedded and heated at 70℃ overnight. The embedded samples were sectioned on a LEICA EM UC7 ultrathin sectioning machine to obtain 70-90 nm sections. Sections were stained with uranyl acetate and lead citrate for 5-10 min each, dried and observed under transmission electron microscopy (HITACHI H-7650).

Mitochondrial membrane potential

The mitochondrial membrane potential of Caco-2 cells was measured using a mitochondrial membrane potential assay kit with JC-1 (Solarbio, Beijing, China). Caco-2 cells were seeded at a density of $2´10^5$ cells/well in laser 24-well plates and cultured for 24 h. After 6 h of exposure to PS, JC-1 solution (20 μg/mL) was added to cells for 20 min. The changes of mitochondrial membrane potential of caco-2 cells were observed by a fluorescence microscope.

Comet assay

Caco-2 cells were seeded at a density of $1´10^6$ cells/well in 6-well plates and cultured for 24 h. After 6 h of exposure to PS, Caco-2 cells were washed twice with medium and digested with trypsin and resuspended in PBS. Mixture of cell suspension (20 μL) of low melting agarose (0.8%, 80 μL) was added to a microscope slide prepared with normal melting agarose (0.5%) layer and covered with a coverslip. After solidification, the coverslips were gently removed, and the slides were immersed in the lysis solution (2.5 M NaCl, 100 mM Na_2EDTA, 10 mM Tris, 200 mM NaOH, 1% Triton X-100, 1% Sodium sarcosinate, pH 10.0) for 90 min at 4 ℃. The slides were washed three times with pre-cooled ultrapure water and then placed on a horizontal electrophoresis device with alkaline electrophoresis buffer (AES: 200 mM NaOH, 1mM Na_2EDTA, pH 13.0) for 30 min at 4 ℃. Electrophoresis was performed for 30 min（25 V, 30 min), and then the slides were rinsed three times with PBS for 5 min. The slides were rinsed with gradients of 50%, 80%, 90% and 100% ethanol for 5 min and then placed in a drying oven for 1 h. Finally, the slides were stained with DAPI (20 μg/mL) and examined under fluorescence microscope.

Apoptosis

Cell apoptosis was detected by Annexin V-FITC/PI Apoptosis Detection Kit (Vazyme, Nanjing, China). Caco-2 cells were seeded at a density of $1´10^6$ cells/well in 6-well plates and cultured for 24 h. After 6 h of exposure to PS, cells were collected with PBS and centrifuged for 5 min at 500×g. After aspirating the supernatant, 500 μL of binding buffer was added to resuspend the cells. 5 μL of Annexin V-FITC and 5 μL of PI were added to cells and mixed sufficiently. A flow cytometry (Backman, USA) was used for apoptosis assay.

PS-MeHg-induced cell viability

Cell viability was detected by CCK-8 kit. Caco-2 cells were seeded at a density of $1´10^5$ cells/well in 96-well plates and cultured for 24 h. Methylmercury chloride (MeHgCl) was purchased from Shanghai Aladdin Biochemical Technology Co. (Aladdin, Shanghai, China). The cells were treated with MeHg (0, 2, 4, 8, 16, 32 and 64 μM) for 6 h. CCK-8 solution (10 μL) was added to each well and incubated for 1 h. The absorbance was measured at 450 nm by a microplate reader. Cell viability was calculated according to absorbance compared with the control group.

To assess the combined toxicity of PS and MeHg on cell. Cell viability was detected by CCK-8 kit. Caco-2 cells were seeded at a density of $1´10^5$ cells/well in 96-well plates and cultured for 24 h. PS20 (20 and 80 μg/mL) and PS200 (20 and 80 μg/mL) were mixed with MeHg (32 μM), respectively, and added to the cells for 6 h incubation. 10 μL of CCK-8 solution was added to each well and incubated for 1 h. Absorbance of the PS-MeHg was measure at 450 nm using a microplate reader. The absorbance of the combination at 600 nm was also measured to eliminate the PS light scattering. Cell viability was calculated based on the relative absorbance compared with the control group.

PS-MeHg-induced apoptosis

Cell apoptosis was detected by Annexin V-FITC/PI Apoptosis Detection Kit. Caco-2 cells were seeded at a density of $1´10^6$ cells/well in 6-well plates and cultured for 24 h. PS and MeHg were diluted with culture medium. After 6 h of exposure to PS-MeHg, cells were collected with PBS and centrifuged for 5 min at 500 g. After aspirating the supernatant, 500 μL of binding buffer was added to resuspend the cells. 5 μL of Annexin V-FITC and 5 μL of PI were added to cells and mixed sufficiently. A flow cytometry was used for apoptosis assay.

Statistical analysis

All data are means ± SEM. Comparisons between the experimental groups and control were performed by oneway ANOVA analysis and least significant difference (LSD) test. A difference was considered significant at $p < 0.05$.

Availability of data and materials

All data generated or analysed during this study are included in this published article and its supplementary information files.

Results

Characterization of PS

The particle size and zeta potential of PS were determined by dynamic light scattering and the results are shown in Table 1. The average sizes of PS20 and PS200 were 29 and 212 nm, respectively. The hydrated particle size of PS in the medium was larger than that in deionized water probably because the nutrients in the medium could attach to their surface [35]. The TEM images clearly revealed that the virgin and fluorescent PS with uniform shape and size (Fig. 1A-D).

Table 1 The hydrodynamic size of PS.

MPs	Medium	Mean diameters [36]	Zeta poential (mV)
PS20	H_2O	29 ± 4	-35 ± 0
	RPMI1640	34 ± 4	-33 ± 2
PS200	H_2O	219 ± 6	-42 ± 1
	RPMI1640	235 ± 3	-31 ± 2

Cell viability

The gastrointestinal tract is an important barrier that blocks MPs from entering human organs. However, recent study showed that MPs can exist in human intestine and can be ingested by the digestive tract [37]. In the present study, Caco-2 cells were employed as a cell model system because their structure and function are similar to the differentiated intestinal epithelial cells. As shown in the Fig. 2A, the relative viability of cells decreased significantly as the concentration of PS20 reached to 80 μg/mL. There was no significant difference in cell viability in PS200 group (Fig. 2B). Therefore, the concentrations of PS used in the further experiments were 20 and 80 μg/mL. PS200 has no cytotoxicity on Caco-2 cells, which was consistent with the result of previous study [38]. Mrakovcic et al. [39] reported that 20 nm PS failed to induce significant cytotoxicity on THP-1 monocytes when the concentration was lower than 50 μg/mL, while the cell viability decreased by 88% at 200 μg/mL.

GSH analysis

As shown in Fig. 2C, both PS20 and PS200 at concentrations of 20 and 80 μg/mL caused a significant decrease in the GSH levels. In all groups, PS20 at 80 μg/mL caused a significantly higher reduction in intracellular GSH content than other treatment groups. GSH has the ability to assist in the conversion of peroxides to less toxic hydroxyl compounds, which can effectively prevent the accumulation of ROS [34]. The decrease of GSH in Caco-2 cells caused by the small size of PS may be one of the reasons for the significant increase of ROS content.

LDH analysis

As depicted in Fig. 2D, compared to untreated cells, no significant LDH leakage was observed in cells treated with PS200. After exposure to 80 μg/mL of PS20, the content of LDH increased sharply, suggesting that the integrity of the cell membrane was disrupted by PS20. In contrast to the results for GSH, leakage of LDH indicates the integrity of the cell membrane as well as the degree of cellular damage. The results for both GSH and LDH indicated that high concentrations of PS20 had the most severe damage on Caco-2 cells.

Intracellular ROS analysis

The ROS production in Caco-2 cells was quantified to determine the effect of PS treatment on oxidative stress of cells. As shown in the Fig. 2E, PS200 at each concentration had no significant effect on ROS production, however the cellular ROS production was dramatically up-regulated by PS20 in a dose-dependent maner. That is to say, PS20 induced more severe oxidative stress than PS200. There is still much controversy regarding the effect of PS on ROS levels. A study showed carboxyl surface-modified and unmodified PS can induce intracellular ROS [40]. However, Li et al. [41] demonstrated that carboxyl-modified polystyrene nanoparticles could effectively inhibit ferroptosis as a result of reduce cellular ROS in RAW264.7 cells. There is still much controversy regarding the effect of PS-induced intracellular ROS levels. To sum up, the results of intracellular ROS effects induced by same surface modified PS is depend on cell types, PS size, and concentration.

Intracellular quantification of PS

The entry of MPs into cells is one of the keys to cause cytotoxicity, and the size is an important property that affects the entry of MPs into cells. The uptake ability of Caco-2 cells to two sizes of PS were investigated in this research. Both 20 nm and 200 nm PS are in the ingestible size range of the cells [42]. Results showed that the uptake of PS of different sizes (20 nm and 200 nm) by Caco-2 cells was significantly different (Fig. 3). After 6h exposure, the uptake rates of 20 nm PS in Caco-2 cells at 20 μg/mL and 80 μg/mL were 63.4% and 96.3%, respectively. For 200 nm, the uptake rates at 20 μg/mL and 80 μg/mL were 22.5% and 20.1%, respectively. The results showed that Caco-2 cells were more efficient in uptake of PS20 than PS200. PS-NPs have been reported to enter in different cell types [43, 44]. Studies have shown that factors affecting the internalization mechanism and uptake efficiency of PS in vitro include the cell type, the size of the PS, and the presence of serum in the culture medium [45]. Dos Santos et al. [46] found that no inhibitor could completely inhibit the uptake of 40 nm and 400 nm PS by the cells. Therefore, the reason for the difference in uptake efficiency of PS20 and PS200 by Caco-2 cells in this study deserves an in-depth study.

Endocytosis of PS by Caco-2 cells

To verify the mechanism by which PS20 and PS200 cause Caco-2 cytotoxicity, we first confirmed the presence of PS20 and PS200 in the cells by TEM analysis and immunofluorescence experiments. As shown in Fig. 4 and video data, fluorescent PS with different sizes were taken up by Caco-2 cells to different degrees after 6 h. Consistent with the results of intracellular quantification of PS, it can be

observed that the amount of internalized PS20 was significantly higher than that of PS200. When the red filter images were merged with green filter images, the position of PS20 was apparent, which revealed that PS20 could enter the cell but the majority were adjacent to cell cytoskeleton. The results of TEM (Fig. 5) assay also confirmed that PS20 and PS200 entered Caco-2 cells and co-localized with mitochondria and endoplasmic reticulum. It predicts that PS20 and PS200 have an effect on the function of organelles such as mitochondria.

Lysosomal tracking of PS

The intracellular localization of PS in lysosomes was detected by organelle specific markers. As shown in Fig. 6, according to merged images, PS20 is more likely to translocate to lysosomes compared to PS200. He et al. [47] documented that endocytic nanoparticles can be transported via the early endosomal/late endosomal/lysosomal pathway. Accumulation of nanoparticles in lysosomes can lead to lysosomal swelling and release of histones into the cytosol, which can further cause to mitochondrial damage and activation of apoptosis [48].

Mitochondrial tracking of PS

As shown in Fig. 7, yellow fluorescence in merge images was an indicator to mitochondrial internalized PS. Due to the different uptake capacity of cells, a higher quantity of PS20 was observed in mitochondria. In addition, we observed a small amount of co-localization of PS200 with mitochondria. Notably, the entry of nanoparticles is harmful to the mitochondria and cause further cytotoxicity [49]. Unlike typical vesicles, mitochondria plays an essential role in intracellular energy supply rather than intracellular transport of macromolecules. He et al. [47] also found that nanopolymers can enter the mitochondria of cells. This result may be related to the non-specific transport pathway of PS20 in cells, which may further induce significant cytotoxicity. Meanwhile, mitochondrial dysfunction is regarded as a main source of ROS production by cells in various pathophysiological states, which may be one of the underlying mechanisms that PS20 at 80 μg/mL induced a large amount of cellular ROS production.

Mitochondrial membrane potential

The decrease of mitochondrial membrane potential is considered to be a marker of early apoptosis [50, 51]. As shown in Fig. 8, the mitochondrial membrane potential of Caco-2 cells was decreased after PS treatment. The fluorogram showed bright green fluorescence after 6 hours of PS20 stimulation of the cells. As the concentration of PS20 increased, the mitochondrial membrane potential decreased to a greater extent. The loss of mitochondrial membrane potential in Caco-2 cells induced by 20 nm PS was significantly greater than that induced by 200 nm.

Comet assay

The comet assay is a validated method for measuring genetic toxicology [52]. As shown in Fig. 9, the nucleus of the control group was intact. However, under treatment of PS, DNA would be damaged into fragments and accumulated in the tail. The length and fragment content of the tail is proportionate to the

degree of DNA damage. Sufficiently small PS can make a direct contact with the nuclear membrane, which can damage DNA and disturb DNA replication [53]. Moreover, indirectly, DNA damage caused by the large amount of cytoplasmic ROS generated by PS through oxidative stress [54].

Apoptosis

Apoptosis was detected using Annexin V-FITV and PI staining, and the results are shown in Fig. 10 and Fig. S2. The results showed that both PS20 at 20 and 80 μg/mL and PS200 in the high concentration group induced apoptosis in Caco-2 cells. At the same concentration, PS20 induced more severe apoptosis in Caco-2 cells than PS200. The late apoptosis rate induced by PS20 at a concentration of 80 μg/mL was significantly higher than that of the low concentration treatment group. To date, most studies have shown that microplastics cause apoptosis in a size- and concentration-dependent manner [32, 55]. However, these studies have focused on large-size or surface-modified microplastics.

PS-MeHg-induced cell viability

As shown in the Fig. 11A, MeHg showed significant cytotoxicity on Caco-2 cells when the concentrations were higher than 32 μg/mL. In further experiments, 32 μg/mL of MeHg was mixed with PS to study the combined toxicity. As depicted in Fig. 10B, PS exerted different effects on the cytotoxicity of MeHg. Briefly, PS20 was incapable of changing the cell viability treated by MeHg. Nevertheless, the adding of PS200 (80 μg/mL) could aggravate the toxicity of MeHg on cells.

PS-MeHg-induced apoptosis

As shown in Fig. 12, PS-MeHg-induced apoptosis was detected by flow cytometry. The apoptosis rate of Caco-2 cells in the presence of MeHg only was 4.02%. Compared to the results of PS-induced apoptosis (Fig. 10 and Fig. S3), the mixture of both sizes of PS with Mehg had a capability to accelerate cell apoptosis. Furthermore, several studies have shown the synergistic toxic effects of MPs and heavy metal [56, 57]. In fact, MPs can act as carriers of heavy metals [58]. Therefore, in this study, the synergistic effect of PS and MeHg may be due to the adsorbance of MeHg to PS and the internalization of PS by cells.

Discussion

The continued use of plastic products will certainly lead to a large accumulation of microplastics in the environment, which is harmful to human health. Previous studies have shown that different types and sizes of PS particles can cause oxidative stress and apoptosis in vitro and in vivo. However, there are few reports on the principles of cell damage caused by PS of such a small size as 20 nm.

In our study, the green fluorescence distribution indicates the entry of PS into Caco-2 cells (Fig. 4, Additional file 2–10). Previously, it was shown that nanoparticles are able to enter cells through phagocytosis, macropinocytosis, as well as clathrin- and caveolae-mediated endocytosis [46, 59]. The red fluorescence representing lysosomes (Fig. 6) and mitochondria (Fig. 7) overlaps with the green

fluorescence of PS, indicating that PS enters the cell and acts further on the organelles. wang et al. [60] showed that amine-modified nano-PS damaged lysosomes during longer incubation times, eventually leading to mitochondrial damage and subsequent activation of apoptosis. After 20 nm PS treatment, Caco-2 cells were in a state of stress and produced an excess of ROS. ROS are capable of oxidizing antioxidant biomolecules, including GSH, so excessive production of ROS is harmful to cells, as evidenced by our experimental results (Fig. 2C, E). The PS-treated cell groups all showed a deficit in mitochondrial membrane potential, which was particularly pronounced in the small size PS group. After cells are stimulated by external stress, the elevation of ROS is accompanied by the generation of pro-apoptotic factors such as the decrease of mitochondrial membrane potential, the opening of mitochondrial membrane permeability transition pore, and the release of cytochrome C, making mitochondria the main executor of apoptotic signals [61, 62]. There is still controversy about the cytotoxic effects of microplastics on heavy metals induced by heavy metals. A part of the voice believes that the presence of microplastics can enhance the toxicity of heavy metals in the environment to the organism [63]. One part of the study showed that the presence of microplastics enhances the toxicity of heavy metals in the environment to the organism. Smaller sized microplastics have a larger specific surface area and can not only interact more with cellular components, but can also adsorb more heavy metals into the cells and thus increase toxicity [64]. The results of another part of the researchers indicate that microplastics can reduce the toxicity of heavy metals [65]. There is an antagonistic effect of microplastics on the cytotoxicity caused by heavy metals due to the adsorption mechanism of heavy metals and the uptake mechanism by cells [66]. In the present study, 20 nm and 200 nm PS had a synergistic effect on the cytotoxicity of MeHg (Fig. 11, 12). In addition, the binding mechanism of PS and MeHg and the PS-MeHg toxicity mechanism need to be studied in depth.

Conclusions

PS20 induced cytotoxicity in a concentration-dependent manner which was determined by cell viability, intracellular ROS levels, and cell membrane integrity. GSH levels indicated that PS200 induced low cellular toxicity. Although Caco-2 cells were able to uptake PS20 and PS200, the quantities of PS20 were higher than PS200 and they aggregated in lysosomes. In addition, because PS20 and PS200 was co-localized with mitochondria, PS20 and PS200 caused depolarization of the mitochondrial membrane potential in Caco-2 cells. Furthermore, PS20 induced more severe apoptosis than PS200. Finally, PS had a synergistic effect in the cytotoxicity of MeHg. Overall, nano-PS induced a stronger effect of decreased viability, mitochondrial damage, apoptosis and synergistic effect with MeHg toxicity in Caco-2 cells than submicron PS. These data are useful for risk assessment of MPs.

Abbreviations

CCK-8: Cell counting kit-8

GSH: Glutathione

LDH: Lactate dehydrogenase

MeHg: Methylmercury

MeHgCl: Methylmercury chloride

MPs: Microplastics

NPs: Nanoplastics

PS: Polystyrene

ROS: Reactive oxygen species

TEM: Transmission Electron Microscope

T-GSH: Total glutathione

Declarations

Acknowledgements

The authors were grateful to all of the laboratory members for their continuous technical advice and helpful discussions.

Funding

This work was supported by Guangdong Yangfan Program (201635018), Guangdong Special Support Program (2017TQ04N706), Science and Technology Planning Project of Zhanjiang City (2018A02014), Industrial Development Special Funds of Dapeng New Area (KY20180202), Guangdong Ocean University Graduate Education Innovation Program Project (202032).

Author information

School of Chemistry and Environment, College of Food Science and Technology, Guangdong Ocean University, Zhanjiang 524088, P.R. China

Zifan Lu, Lei He, Chunxia Zhou, Pengzhi Hong, Zhong-Ji Qian, Xianghong Ju, Shengli Sun & Chengyong Li

Shenzhen Institute of Guangdong Ocean University, Shenzhen, Guangdong 518114, P.R. China

Yuanyuan Zhang, Lei He, Chunxia Zhou, Pengzhi Hong, Zhong-Ji Qian, Xianghong Ju & Chengyong Li

Contributions

Zifan Lu: study design, perform experiments, data analysis, original draft preparation; Yuanyuan Zhang: manuscript preparation. Lei He: writing - review & editing; Chunxia Zhou: software; Pengzhi Hong: Project administration; Zhong-Ji Qian: study design; Xianghong Ju: supervision; Shengli Sun: manuscript preparation; Chengyong Li: study design, funding.

Corresponding authors

Correspondence to Chengyong Li.

Ethics declarations

Ethics approval and consent to participate

Not applicable.

Consent for publication

All authors have given approval to the final version of the manuscript.

Competing interests

The authors declare no competing financial interests.

References

1. Auffan M, Rose J, Bottero J-Y, Lowry GV, Jolivet J-P, Wiesner MR. Towards a definition of inorganic nanoparticles from an environmental, health and safety perspective. Nature Nanotechnology. 2009;4 10:634–41; doi: 10.1038/nnano.2009.242.
2. Peng X, Chen M, Chen S, Dasgupta S, Xu H, Ta K, et al. Microplastics contaminate the deepest part of the world's ocean. Geochemical Perspectives Letters. 2018:1–5; doi: 10.7185/geochemlet.1829.
3. Napper IE, Davies BFR, Clifford H, Elvin S, Koldewey HJ, Mayewski PA, et al. Reaching New Heights in Plastic Pollution—Preliminary Findings of Microplastics on Mount Everest. One Earth. 2020;3 5:621–30; doi: https://doi.org/10.1016/j.oneear.2020.10.020.
4. Jambeck JR, Geyer R, Wilcox C, Siegler TR, Perryman M, Andrady A, et al. Plastic waste inputs from land into the ocean. Science. 2015;347 6223:768–71; doi: 10.1126/science.1260352.
5. Jiang S, Zhang Y, Feng L, He L, Zhou C, Hong P, et al. Comparison of Short- and Long-Term Toxicity of Microplastics with Different Chemical Constituents on Button Polyps. (Protopalythoa sp.). ACS Earth and Space Chemistry. 2021;5 1:12–22; doi: 10.1021/acsearthspacechem.0c00213.
6. Feng L, He L, Jiang S, Chen J, Zhou C, Qian Z-J, et al. Investigating the composition and distribution of microplastics surface biofilms in coral areas. Chemosphere. 2020;252:126565; doi: https://doi.org/10.1016/j.chemosphere.2020.126565.

7. Renzi M, Blašković A. Litter & microplastics features in table salts from marine origin: Italian versus Croatian brands. Marine Pollution Bulletin. 2018;135:62 – 8; doi: https://doi.org/10.1016/j.marpolbul.2018.06.065.
8. Cho Y, Shim WJ, Jang M, Han GM, Hong SH. Abundance and characteristics of microplastics in market bivalves from South Korea. Environmental Pollution. 2019;245:1107–16; doi: 10.1016/j.envpol.2018.11.091.
9. Karami A, Golieskardi A, Choo CK, Larat V, Karbalaei S, Salamatinia B. Microplastic and mesoplastic contamination in canned sardines and sprats. Sci Total Environ. 2018;612:1380–6; doi: https://doi.org/10.1016/j.scitotenv.2017.09.005.
10. Liebezeit G, Liebezeit E. Non-pollen particulates in honey and sugar. Food Additives & Contaminants: Part A. 2013;30 12:2136–40; doi: 10.1080/19440049.2013.843025.
11. Hernandez LM, Xu EG, Larsson HCE, Tahara R, Maisuria VB, Tufenkji N. Plastic Teabags Release Billions of Microparticles and Nanoparticles into Tea. Environ Sci Technol. 2019;53 21:12300–10; doi: 10.1021/acs.est.9b02540.
12. Lindeque PK, Cole M, Coppock RL, Lewis CN, Miller RZ, Watts AJR, et al. Are we underestimating microplastic abundance in the marine environment? A comparison of microplastic capture with nets of different mesh-size. Environmental Pollution. 2020;265:12; doi: 10.1016/j.envpol.2020.114721.
13. Daniel DB, Ashraf PM, Thomas SN, Thomson KT. Microplastics in the edible tissues of shellfishes sold for human consumption. Chemosphere. 2021;264:9; doi: 10.1016/j.chemosphere.2020.128554.
14. Teng J, Wang Q, Ran W, Wu D, Liu YF, Sun S, et al. Microplastic in cultured oysters from different coastal areas of China. Sci Total Environ. 2019;653:1282–92; doi: 10.1016/j.scitotenv.2018.11.057.
15. Huerta Lwanga E, Mendoza Vega J, Ku Quej V, Chi JdlA, Sanchez del Cid L, Chi C, et al. Field evidence for transfer of plastic debris along a terrestrial food chain. Scientific Reports. 2017;7 1:14071; doi: 10.1038/s41598-017-14588-2.
16. Lv L, He L, Jiang S, Chen J, Zhou C, Qu J, et al. In situ surface-enhanced Raman spectroscopy for detecting microplastics and nanoplastics in aquatic environments. Sci Total Environ. 2020;728:138449; doi: https://doi.org/10.1016/j.scitotenv.2020.138449.
17. Koelmans AA, Bakir A, Burton GA, Janssen CR. Microplastic as a Vector for Chemicals in the Aquatic Environment: Critical Review and Model-Supported Reinterpretation of Empirical Studies. Environ Sci Technol. 2016;50 7:3315–26; doi: 10.1021/acs.est.5b06069.
18. Turner A, Holmes LA. Adsorption of trace metals by microplastic pellets in fresh water. Environ Chem. 2015;12 5:600–10; doi: 10.1071/en14143.
19. Bohn P, Bak SA, Bjorklund E, Krogh KA, Hansen M. Abiotic degradation of antibiotic ionophores. Environmental Pollution. 2013;182:177–83; doi: 10.1016/j.envpol.2013.06.040.
20. Xie H, Chen J, Feng L, He L, Zhou C, Hong P, et al. Chemotaxis-selective colonization of mangrove rhizosphere microbes on nine different microplastics. Sci Total Environ. 2021;752:142223; doi: https://doi.org/10.1016/j.scitotenv.2020.142223.

21. Gasperi J, Wright SL, Dris R, Collard F, Mandin C, Guerrouache M, et al. Microplastics in air: Are we breathing it in? Current Opinion in Environmental Science & Health. 2018;1:1–5; doi: https://doi.org/10.1016/j.coesh.2017.10.002.
22. Galloway TS. Micro- and Nano-plastics and Human Health. In: Bergmann M, Gutow L, Klages M, editors. Marine Anthropogenic Litter. Cham: Springer International Publishing; 2015. p. 343–66.
23. Reinholz J, Diesler C, Schöttler S, Kokkinopoulou M, Ritz S, Landfester K, et al. Protein machineries defining pathways of nanocarrier exocytosis and transcytosis. Acta Biomaterialia. 2018;71:432–43; doi: https://doi.org/10.1016/j.actbio.2018.03.006.
24. Anselmo AC, Gupta V, Zern BJ, Pan D, Zakrewsky M, Muzykantov V, et al. Delivering Nanoparticles to Lungs while Avoiding Liver and Spleen through Adsorption on Red Blood Cells. ACS Nano. 2013;7 12:11129–37; doi: 10.1021/nn404853z.
25. Chambers E, Mitragotri S. Prolonged circulation of large polymeric nanoparticles by non-covalent adsorption on erythrocytes. J Control Release. 2004;100 1:111–9; doi: 10.1016/j.jconrel.2004.08.005.
26. Wick P, Malek A, Manser P, Meili D, Maeder-Althaus X, Diener L, et al. Barrier Capacity of Human Placenta for Nanosized Materials. Environmental Health Perspectives. 2010;118 3:432–6; doi: 10.1289/ehp.0901200.
27. Yang CS, Chang CH, Tsai PJ, Chen WY, Tseng FG, Lo LW. Nanoparticle-based in vivo investigation on blood-brain barrier permeability following ischemia and reperfusion. Anal Chem. 2004;76 15:4465–71; doi: 10.1021/ac035491v.
28. Brown DM, Wilson MR, MacNee W, Stone V, Donaldson K. Size-dependent proinflammatory effects of ultrafine polystyrene particles: a role for surface area and oxidative stress in the enhanced activity of ultrafines. Toxicol Appl Pharmacol. 2001;175 3:191–9; doi: 10.1006/taap.2001.9240.
29. Forte M, Iachetta G, Tussellino M, Carotenuto R, Prisco M, De Falco M, et al. Polystyrene nanoparticles internalization in human gastric adenocarcinoma cells. Toxicol Vitro. 2016;31:126–36; doi: https://doi.org/10.1016/j.tiv.2015.11.006.
30. Xu MK, Halimu G, Zhang QR, Song YB, Fu XH, Li YQ, et al. Internalization and toxicity: A preliminary study of effects of nanoplastic particles on human lung epithelial cell. Sci Total Environ. 2019;694:10; doi: 10.1016/j.scitotenv.2019.133794.
31. Lehner R, Weder C, Petri-Fink A, Rothen-Rutishauser B. Emergence of Nanoplastic in the Environment and Possible Impact on Human Health. Environ Sci Technol. 2019;53 4:1748–65; doi: 10.1021/acs.est.8b05512.
32. Kulkarni SA, Feng S-S. Effects of Particle Size and Surface Modification on Cellular Uptake and Biodistribution of Polymeric Nanoparticles for Drug Delivery. Pharm Res. 2013;30 10:2512–22; doi: 10.1007/s11095-012-0958-3.
33. Wang Q, Bai J, Ning B, Fan L, Sun T, Fang Y, et al. Effects of bisphenol A and nanoscale and microscale polystyrene plastic exposure on particle uptake and toxicity in human Caco-2 cells. Chemosphere. 2020;254:126788; doi: 10.1016/j.chemosphere.2020.126788.

34. Jiang Y, Tang X, Zhou B, Sun T, Chen H, Zhao X, et al. The ROS-mediated pathway coupled with the MAPK-p38 signalling pathway and antioxidant system plays roles in the responses of Mytilus edulis haemocytes induced by BDE-47. Aquatic Toxicology. 2017;187:55–63; doi: https://doi.org/10.1016/j.aquatox.2017.03.011.
35. Yan XM, Zhang YY, Lu YQ, He L, Qu JH, Zhou CX, et al. The Complex Toxicity of Tetracycline with Polystyrene Spheres on Gastric Cancer Cells. Int J Environ Res Public Health. 2020;17 8:14; doi: 10.3390/ijerph17082808.
36. Stock V, Laurisch C, Franke J, Donmez MH, Voss L, Bohmert L, et al. Uptake and cellular effects of PE, PP, PET and PVC microplastic particles. Toxicol Vitro. 2021;70:9; doi: 10.1016/j.tiv.2020.105021.
37. Ibrahim YS, Tuan Anuar S, Azmi AA, Wan Mohd Khalik WMA, Lehata S, Hamzah SR, et al. Detection of microplastics in human colectomy specimens. JGH Open. 2021;5 1:116–21; doi: 10.1002/jgh3.12457.
38. Behrens I, Pena AIV, Alonso MJ, Kissel T. Comparative uptake studies of bioadhesive and non-bioadhesive nanoparticles in human intestinal cell lines and rats: The effect of mucus on particle adsorption and transport. Pharm Res. 2002;19 8:1185–93; doi: 10.1023/a:1019854327540.
39. Mrakovcic M, Meindl C, Roblegg E, Froehlich E. Reaction of monocytes to polystyrene and silica nanoparticles in short-term and long-term exposures. Toxicology Research. 2014;3 2:86–97; doi: 10.1039/c3tx50112d.
40. He Y, Li J, Chen J, Miao X, Li G, He Q, et al. Cytotoxic effects of polystyrene nanoplastics with different surface functionalization on human HepG2 cells. Sci Total Environ. 2020;723:138180; doi: https://doi.org/10.1016/j.scitotenv.2020.138180.
41. Li L, Sun SL, Tan LL, Wang YF, Wang LY, Zhang ZR, et al. Polystyrene Nanoparticles Reduced ROS and Inhibited Ferroptosis by Triggering Lysosome Stress and TFEB Nucleus Translocation in a Size-Dependent Manner. Nano Lett. 2019;19 11:7781–92; doi: 10.1021/acs.nanolett.9b02795.
42. Bruinink A, Wang J, Wick P. Effect of particle agglomeration in nanotoxicology. Arch Toxicol. 2015;89 5:659–75; doi: 10.1007/s00204-015-1460-6.
43. Johnston HJ, Semmler-Behnke M, Brown DM, Kreyling W, Tran L, Stone V. Evaluating the uptake and intracellular fate of polystyrene nanoparticles by primary and hepatocyte cell lines in vitro. Toxicol Appl Pharmacol. 2010;242 1:66–78; doi: 10.1016/j.taap.2009.09.015.
44. Geys J, Coenegrachts L, Vercammen J, Engelborghs Y, Nemmar A, Nemery B, et al. In vitro study of the pulmonary translocation of nanoparticles - A preliminary study. Toxicol Lett. 2006;160 3:218–26; doi: 10.1016/j.toxlet.2005.07.005.
45. Smith PJ, Giroud M, Wiggins HL, Gower F, Thorley JA, Stolpe B, et al. Cellular entry of nanoparticles via serum sensitive clathrin-mediated endocytosis, and plasma membrane permeabilization. Int J Nanomed. 2012;7:2045–55; doi: 10.2147/ijn.S29334.
46. dos Santos T, Varela J, Lynch I, Salvati A, Dawson KA. Effects of Transport Inhibitors on the Cellular Uptake of Carboxylated Polystyrene Nanoparticles in Different Cell Lines. PLoS One. 2011;6 9:10; doi: 10.1371/journal.pone.0024438.

47. He B, Lin P, Jia Z, Du W, Qu W, Yuan L, et al. The transport mechanisms of polymer nanoparticles in Caco-2 epithelial cells. Biomaterials. 2013;34 25:6082–98; doi: https://doi.org/10.1016/j.biomaterials.2013.04.053.
48. Wu B, Torres-Duarte C, Cole BJ, Cherr GN. Copper Oxide and Zinc Oxide Nanomaterials Act as Inhibitors of Multidrug Resistance Transport in Sea Urchin Embryos: Their Role as Chemosensitizers. Environ Sci Technol. 2015;49 9:5760–70; doi: 10.1021/acs.est.5b00345.
49. Salnikov V, Lukyánenko YO, Frederick CA, Lederer WJ, Lukyánenko V. Probing the Outer Mitochondrial Membrane in Cardiac Mitochondria with Nanoparticles. Biophysical Journal. 2007;92 3:1058–71; doi: https://doi.org/10.1529/biophysj.106.094318.
50. Kroemer G, Dallaporta B, Resche-Rigon M. The mitochondrial death/life regulator in apoptosis and necrosis. Annual review of physiology. 1998;60:619–42; doi: 10.1146/annurev.physiol.60.1.619.
51. Reed JC, Green DR. Remodeling for demolition: Changes in mitochrondrial ultrastructure during apoptosis. Molecular Cell. 2002;9 1:1–3; doi: 10.1016/s1097-2765(02)00437-9.
52. Azqueta A, Dusinska M. The use of the comet assay for the evaluation of the genotoxicity of nanomaterials. Front Genet. 2015;6:4; doi: 10.3389/fgene.2015.00239.
53. Kihara S, Ashenden A, Kaur M, Glasson J, Ghosh S, van der Heijden N, et al. Cellular interactions with polystyrene nanoplastics-The role of particle size and protein corona. BIOINTERPHASES. 2021;16 4; doi: 10.1116/6.0001124.
54. Howard J, Murashov V. Adverse Effects of Engineered Nanomaterials Exposure, Toxicology, and Impact on Human Health. Journal of Occupational & Environmental Medicine. 2013;55 6:722–3; doi: 10.1097/JOM.0b013e3182882c46.
55. Jung BK, Han SW, Park SH, Bae JS, Choi J, Ryu KY. Neurotoxic potential of polystyrene nanoplastics in primary cells originating from mouse brain. Neurotoxicology. 2020;81:189–96; doi: 10.1016/j.neuro.2020.10.008.
56. Banaee M, Soltanian S, Sureda A, Gholamhosseini A, Haghi BN, Akhlaghi M, et al. Evaluation of single and combined effects of cadmium and micro-plastic particles on biochemical and immunological parameters of common carp (Cyprinus carpio). Chemosphere. 2019;236:11; doi: 10.1016/j.chemosphere.2019.07.066.
57. Dong YM, Gao ML, Song ZG, Qiu WW. Microplastic particles increase arsenic toxicity to rice seedlings. Environmental Pollution. 2020;259:11; doi: 10.1016/j.envpol.2019.113892.
58. Massos A, Turner A. Cadmium, lead and bromine in beached microplastics. Environmental Pollution. 2017;227:139–45; doi: 10.1016/j.envpol.2017.04.034.
59. Fiorentino I, Gualtieri R, Barbato V, Mollo V, Braun S, Angrisani A, et al. Energy independent uptake and release of polystyrene nanoparticles in primary mammalian cell cultures. EXPERIMENTAL CELL RESEARCH. 2015;330 2:240–7; doi: 10.1016/j.yexcr.2014.09.017.
60. Wang FJ, Bexiga MG, Anguissola S, Boya P, Simpson JC, Salvati A, et al. Time resolved study of cell death mechanisms induced by amine-modified polystyrene nanoparticles. NANOSCALE. 2013;5 22:10868–76; doi: 10.1039/c3nr03249c.

61. Iverson SL, Orrenius S. The cardiolipin-cytochromet c interaction and the mitochondrial regulation of apoptosis. ARCHIVES OF BIOCHEMISTRY AND BIOPHYSICS. 2004;423 1:37–46; doi: 10.1016/j.abb.2003.12.002.
62. Green DR, Kroemer G. The pathophysiology of mitochondrial cell death. Science. 2004;305 5684:626–9; doi: 10.1126/science.1099320.
63. Bhagat J, Nishimura N, Shimada Y. Toxicological interactions of microplastics/nanoplastics and environmental contaminants: Current knowledge and future perspectives. Journal of Hazardous Materials. 2021;405:123913; doi: https://doi.org/10.1016/j.jhazmat.2020.123913.
64. Zhang F, Wang Z, Song L, Fang H, Wang DG. Aquatic toxicity of iron-oxide-doped microplastics to Chlorella pyrenoidosa and Daphnia magna. ENVIRONMENTAL POLLUTION. 2020;257; doi: 10.1016/j.envpol.2019.113451.
65. Pacheco A, Martins A, Guilhermino L. Toxicological interactions induced by chronic exposure to gold nanoparticles and microplastics mixtures in Daphnia magna. Sci Total Environ. 2018;628–629:474 – 83; doi: 10.1016/j.scitotenv.2018.02.081.
66. Miranda T, Vieira LR, Guilhermino L. Neurotoxicity, Behavior, and Lethal Effects of Cadmium, Microplastics, and Their Mixtures on Pomatoschistus microps Juveniles from Two Wild Populations Exposed under Laboratory Conditions?Implications to Environmental and Human Risk Assessment. Int J Environ Res Public Health. 2019;16 16; doi: 10.3390/ijerph16162857.

Figures

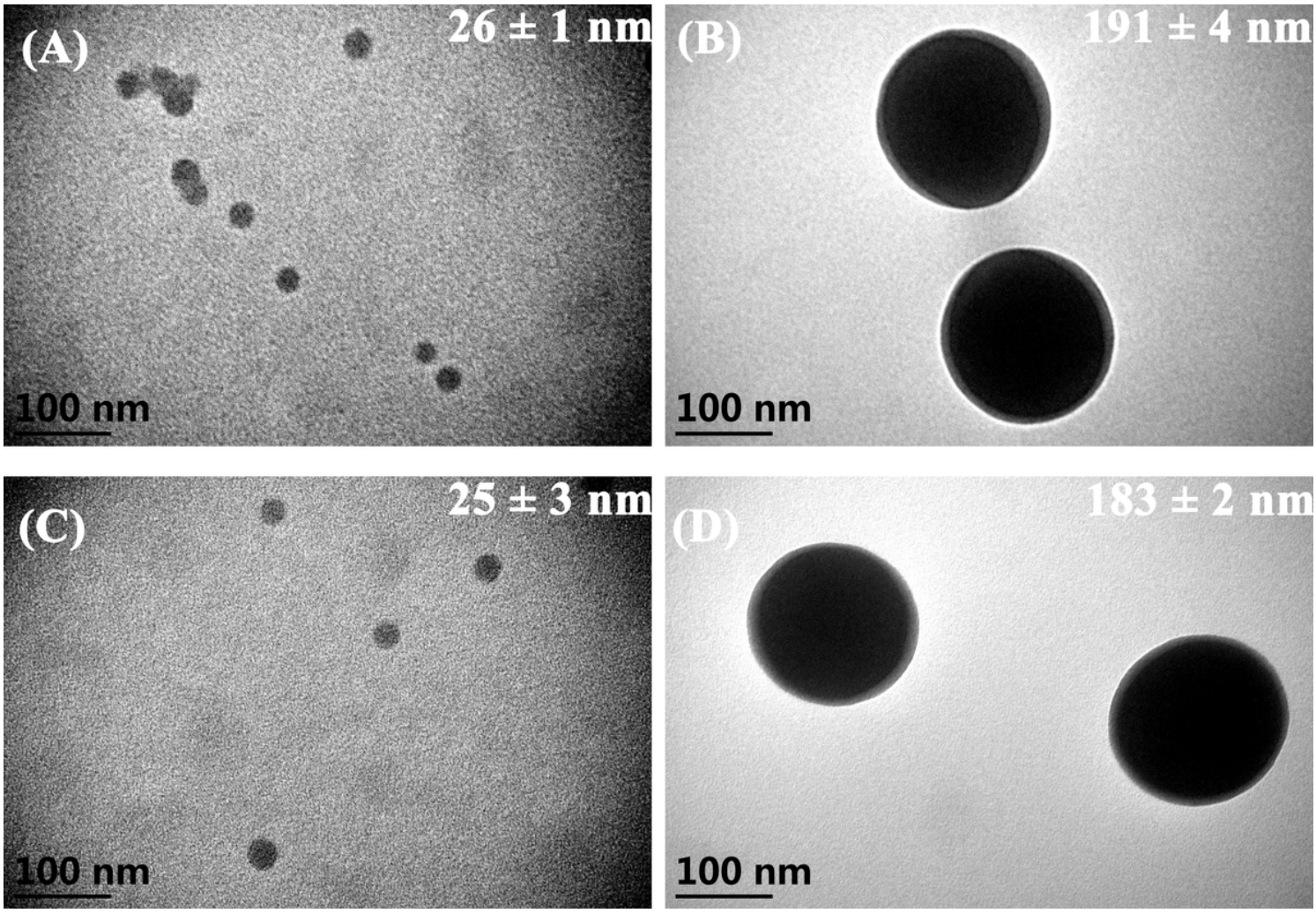

Figure 1

Characterization of PS microplastics. (A) TEM image of PS20; (B) TEM image of PS200; (C) TEM image of fluorescent PS20; (D) TEM image of fluorescent PS200.

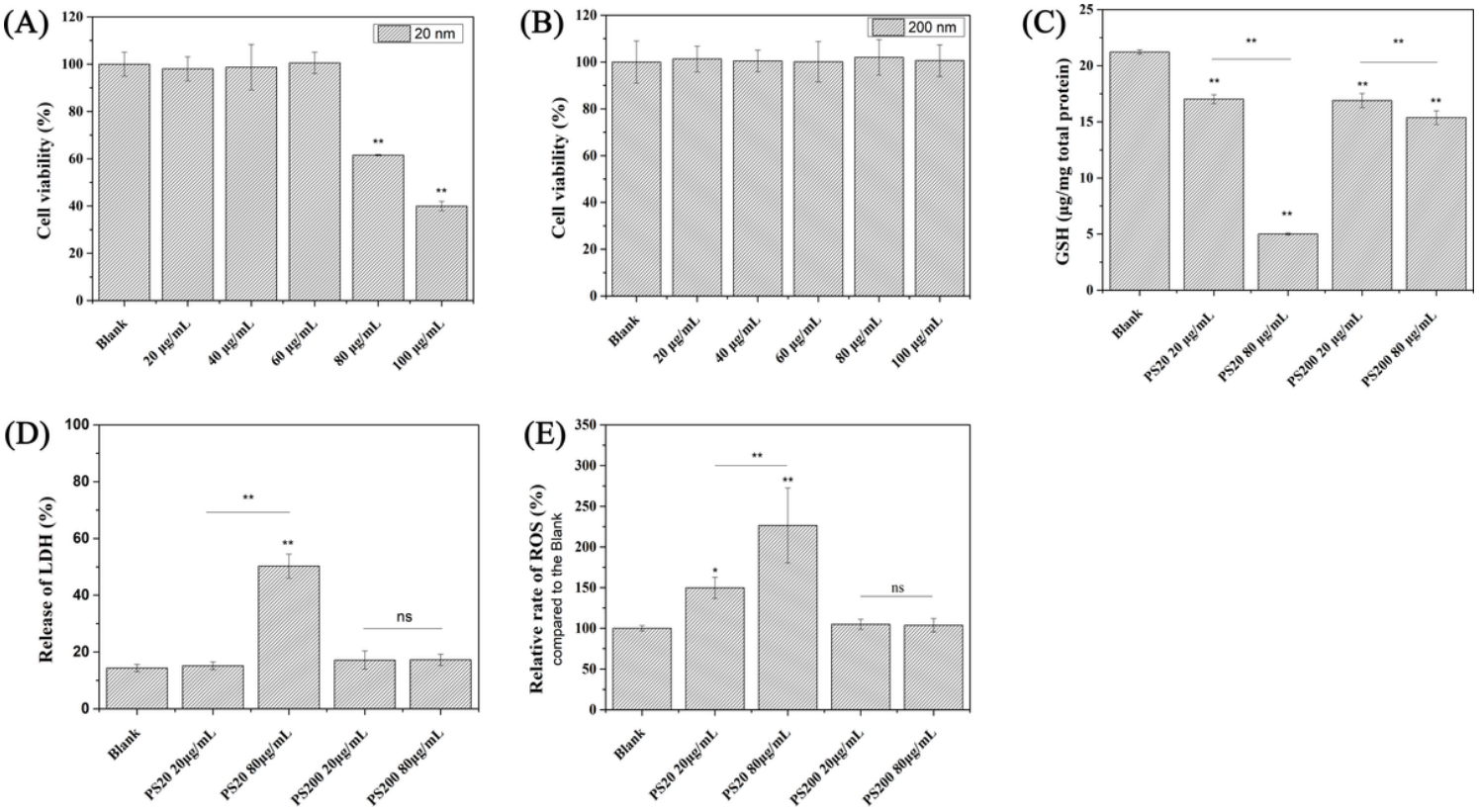

Figure 2

Cytotoxicity induced by PS20 and PS200. (A) and (B) Cell viability after 6 h exposure to PS20 and PS200, respectively. (C) GSH after 6h exposure to PS20 and PS200. (D) and (E) The relative LDH release values and ROS levels induced by PS20 and PS200, respectively. (*$p < 0.05$, **$p < 0.01$)

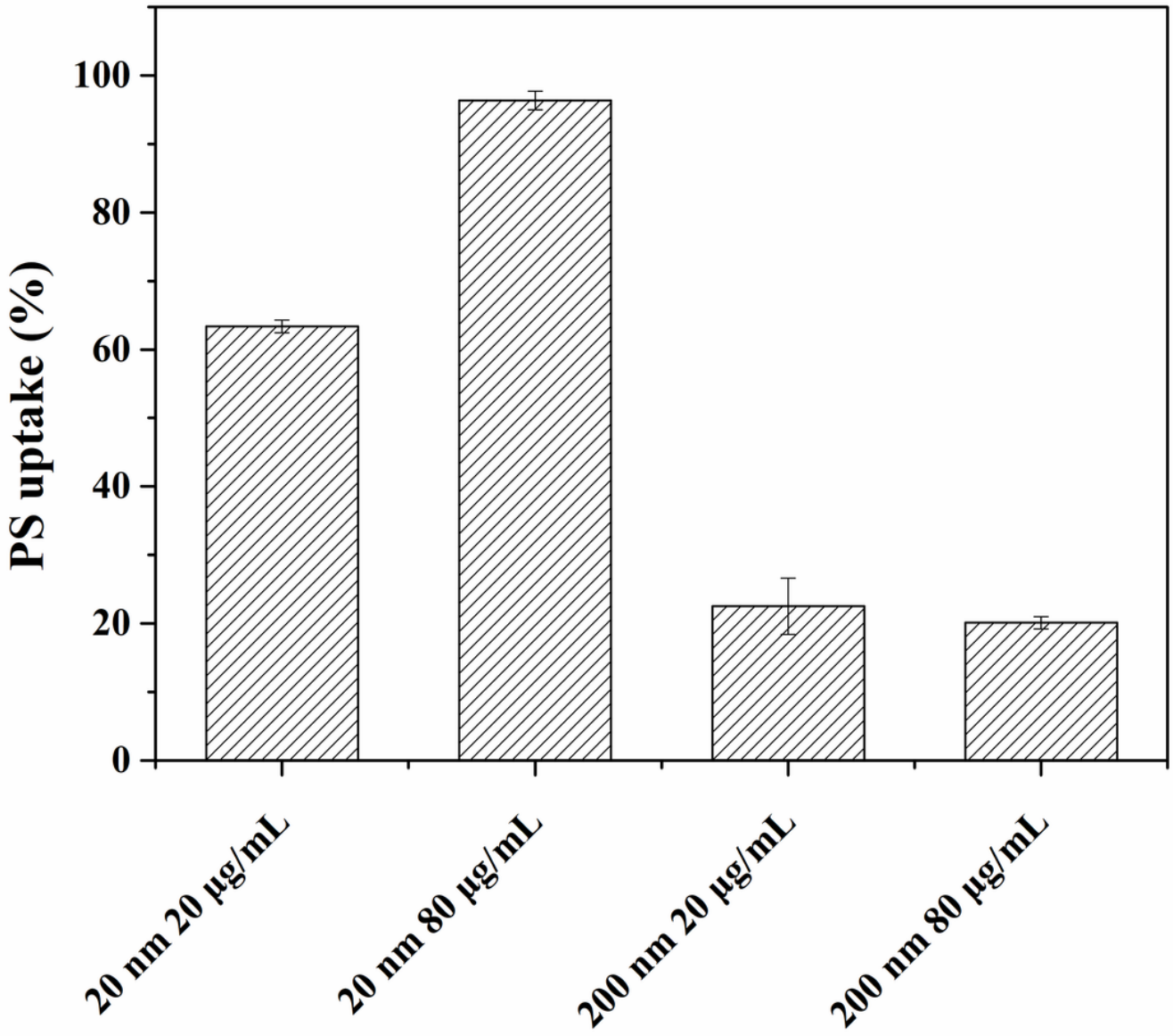

Figure 3

Uptake of PS in Caco-2 cells for 6 h.

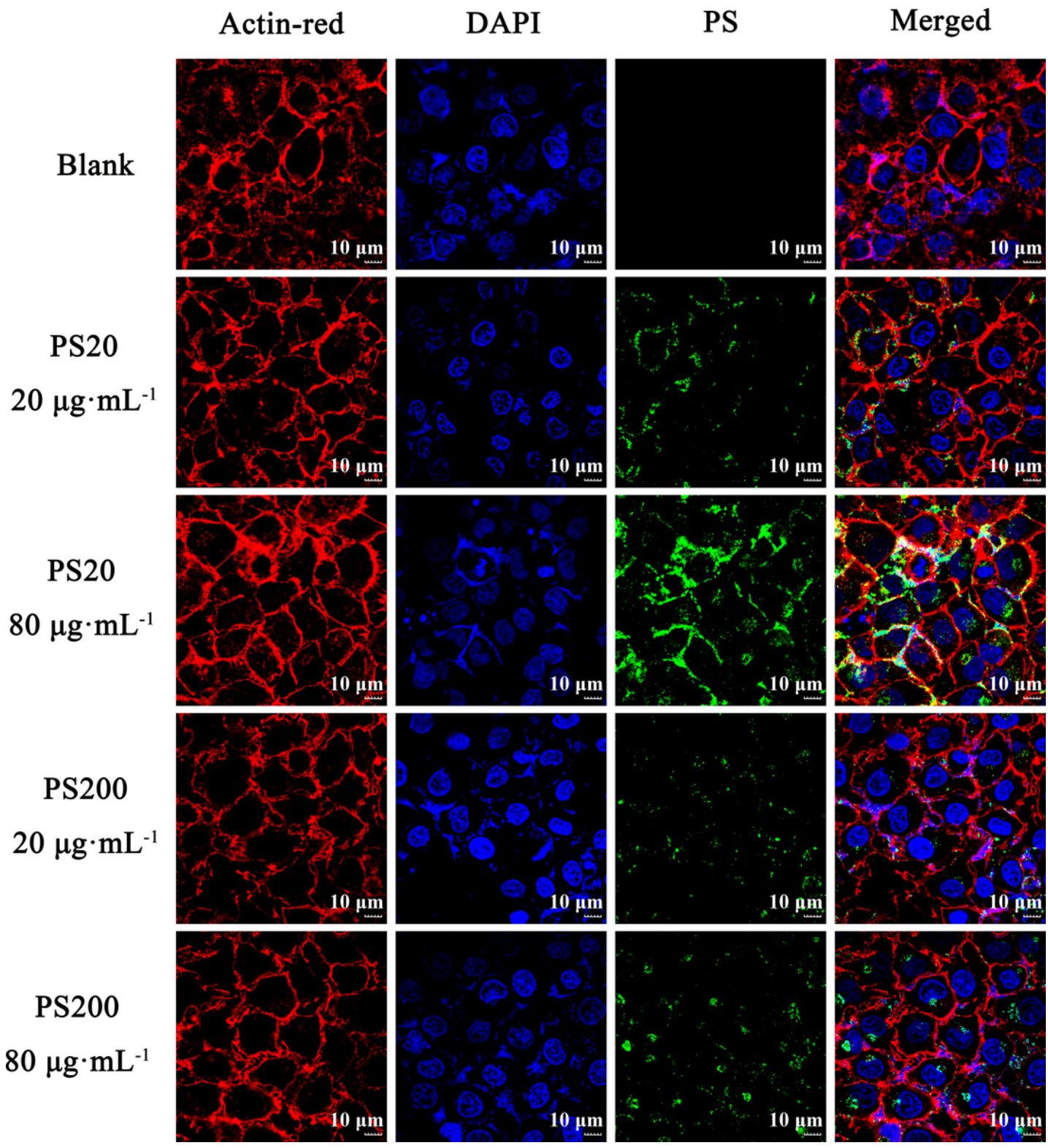

Figure 4

Confocal laser scanning images of Caco-2 cells incubated with green fluorescent PS for 6 hours. Actin was stained with Actin-Red (red). Cell nuclei were stained with DAPI (blue).

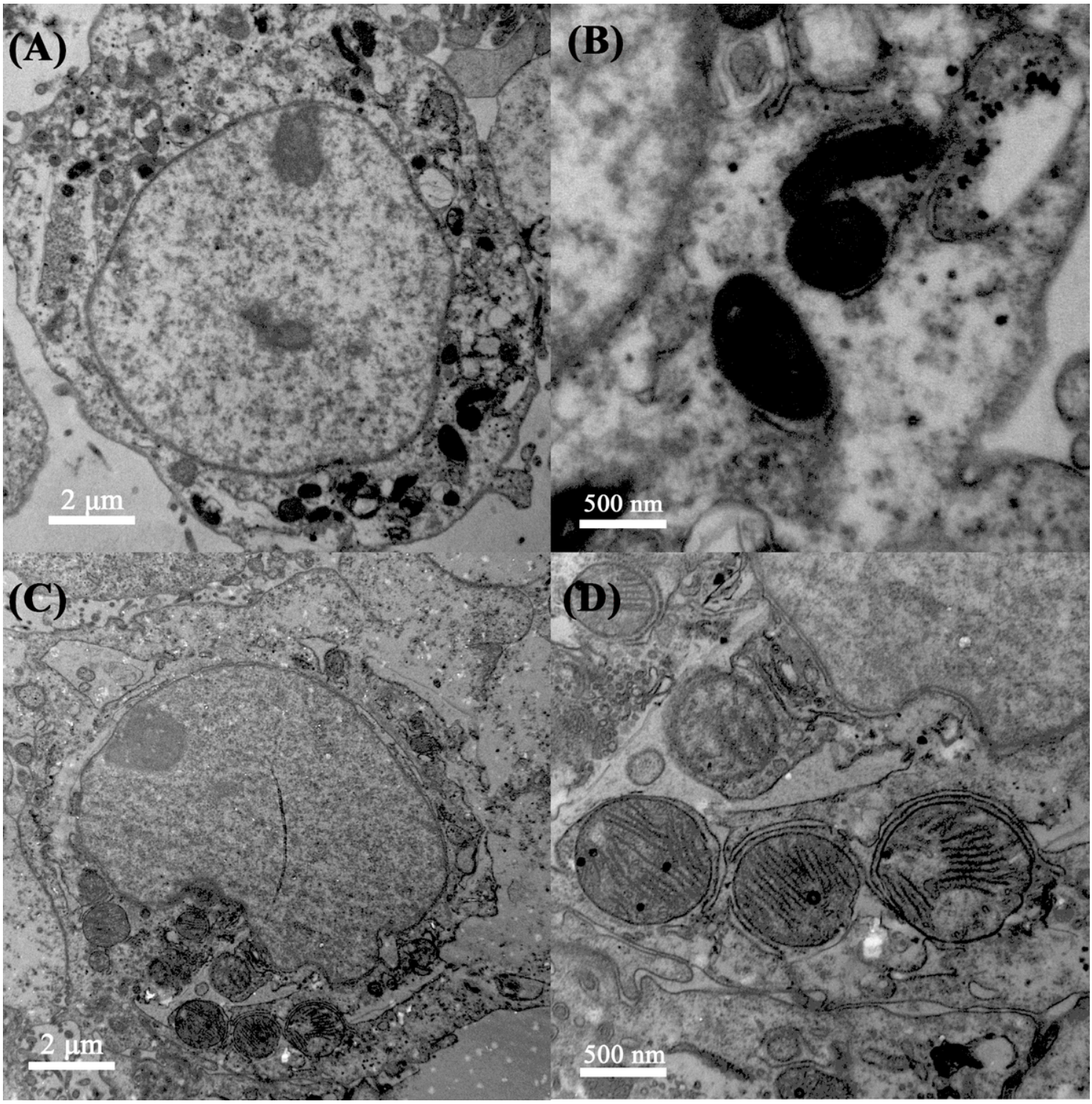

Figure 5

TEM analysis of endocytosis of PS by Caco-2 cells. (A) and (B) The endocytosis of PS20 by Caco-2 cells. (C) and (D) The endocytosis of PS200 by Caco-2 cells.

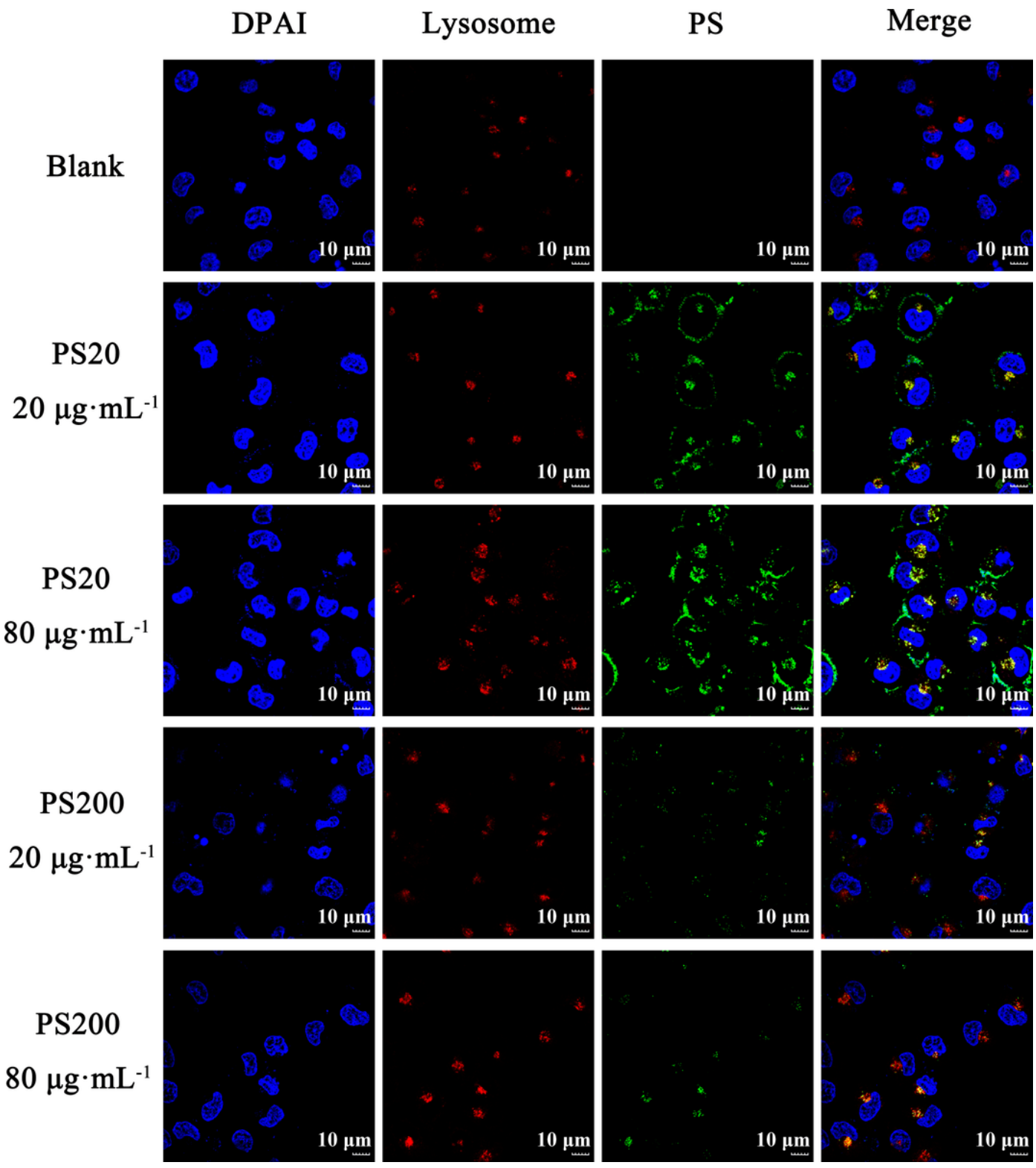

Figure 6

Confocal laser scanning microscope images of Caco-2 cells incubated for 6 h with green fluorescent PS. Lysosomes were stained with LysoTracker Red (red). Cell nuclei were stained with DAPI (blue).

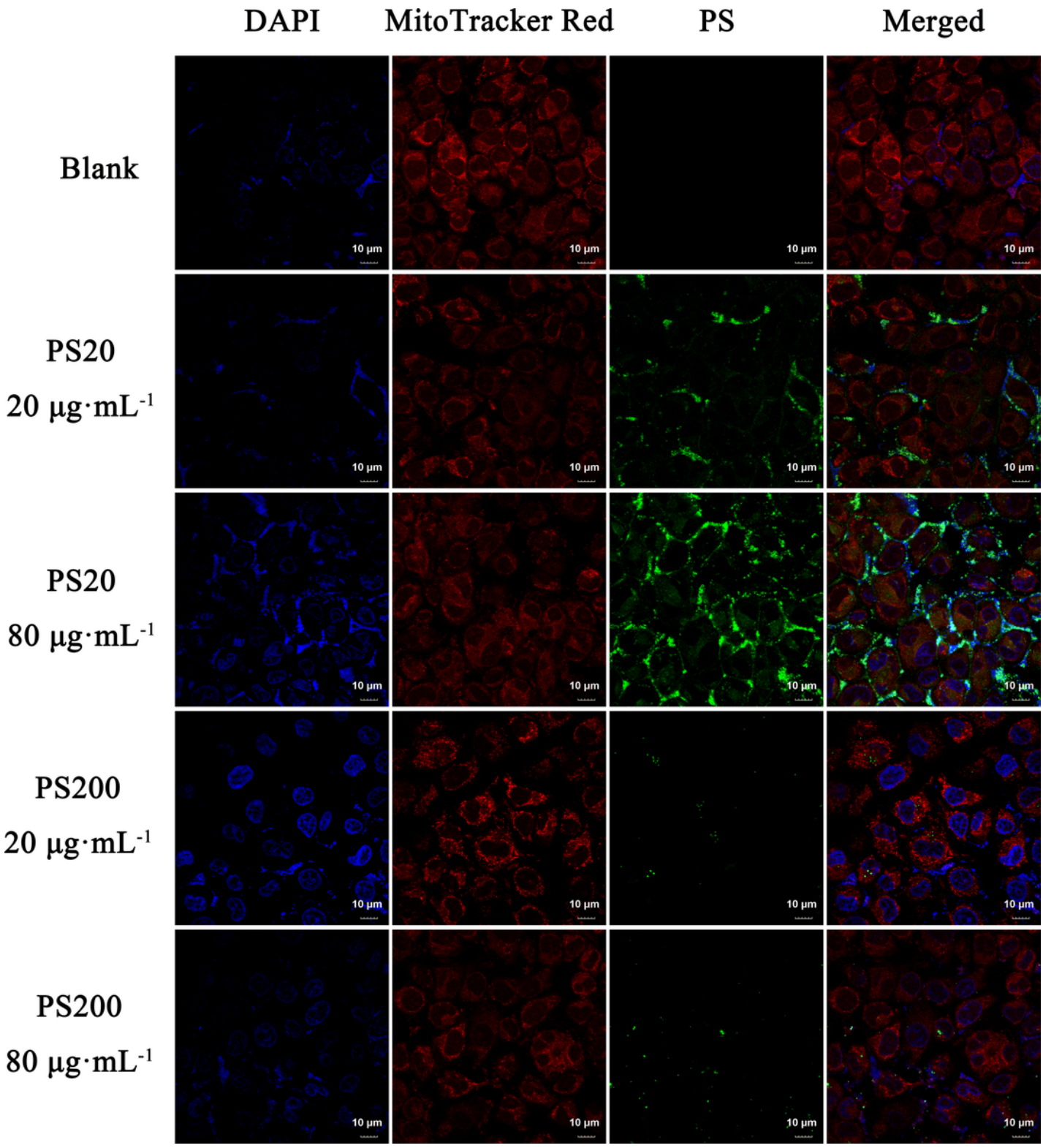

Figure 7

Confocal laser scanning microscope images of Caco-2 cells incubated for 6 h with green fluorescent PS. Mitochondria were stained with MitoTracker Red (red). Cell nuclei were stained with DAPI (blue).

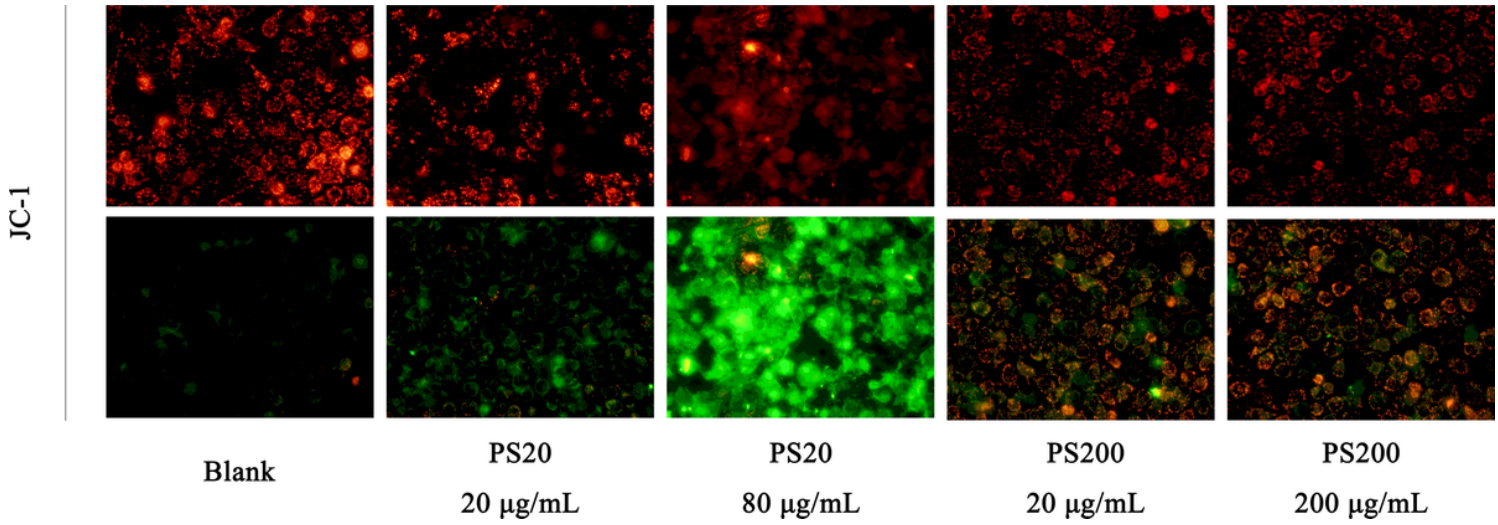

Figure 8

Effect of PS on the mitochondrial membrane potential of Caco-2 cells (20´). Red to green fluorescence shift indicates a decrease in mitochondrial membrane potential.

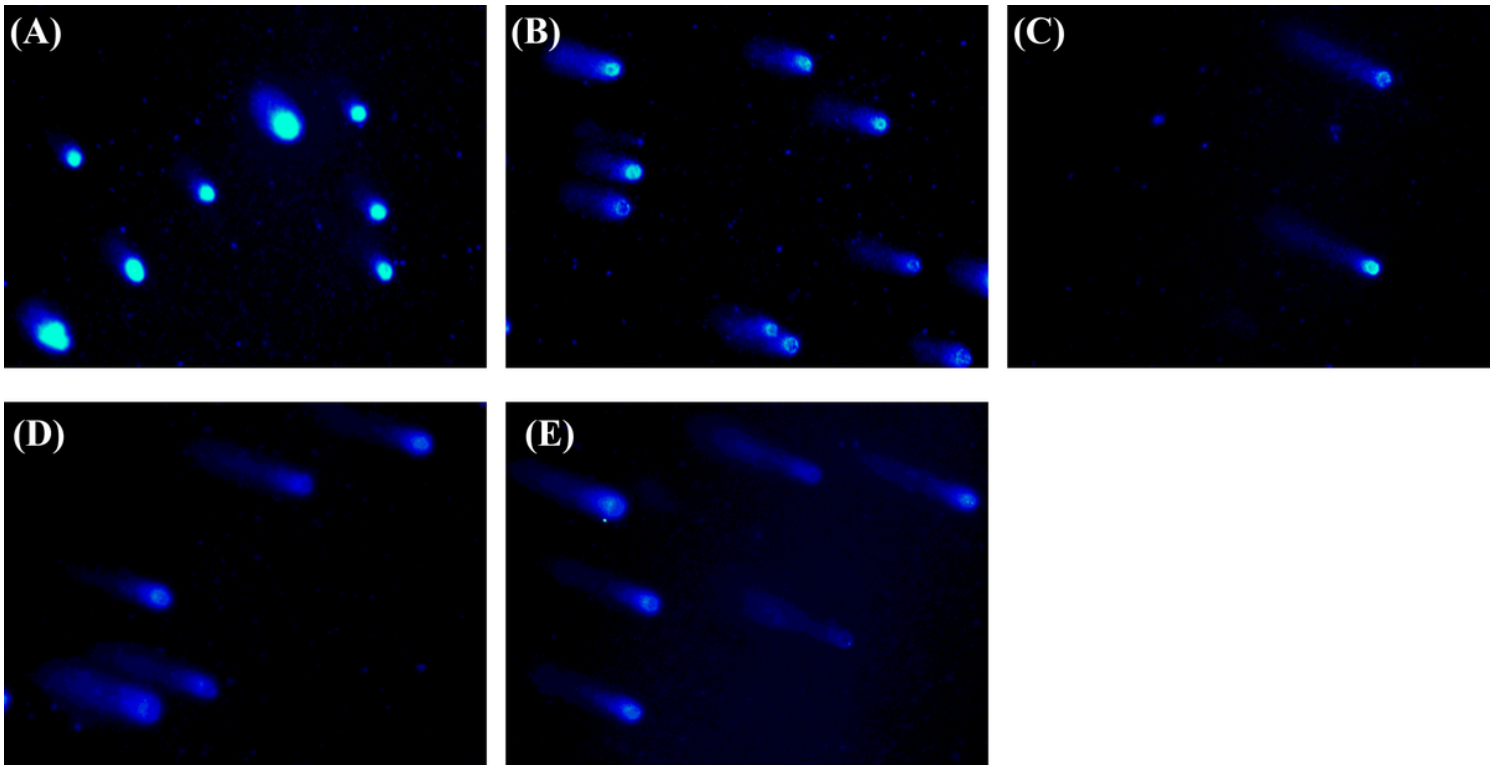

Figure 9

PS-induced DNA damage in Caco-2 cells. (A) Control group (40´). (B) 20 μg/mL of PS20 (40´). (C) 80 μg/mL of PS20 (40´). (D) 20 μg/mL of PS200 (40´). (E) 80 μg/mL of PS200 (40´).

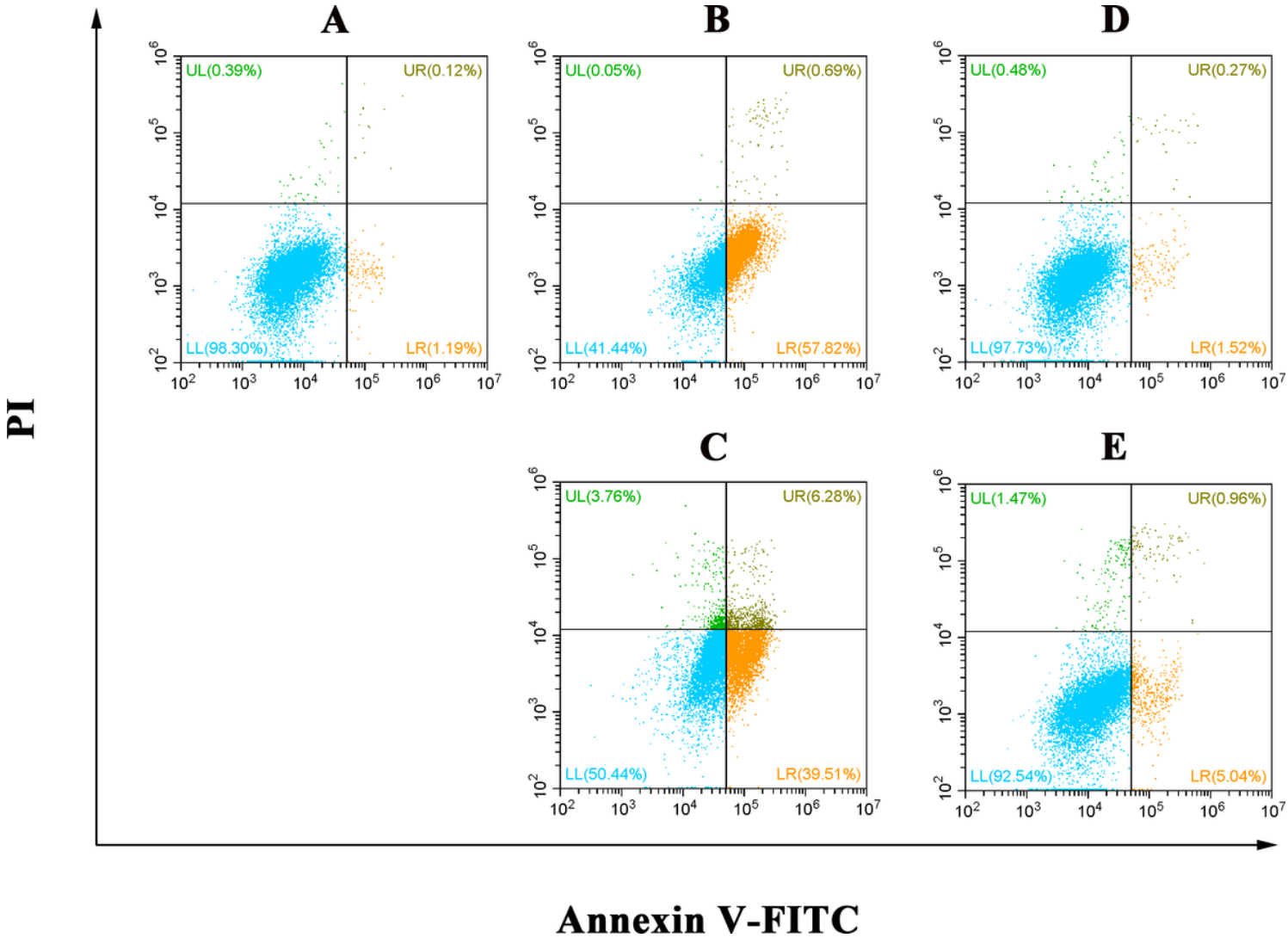

Figure 10

Effect of PS on apoptosis of Caco-2 cells. (A) Control group. (B) 20 μg/mL of PS20. (C) 80 μg/mL of PS20. (D) 20 μg/mL of PS200. (E) 80 μg/mL of PS200.

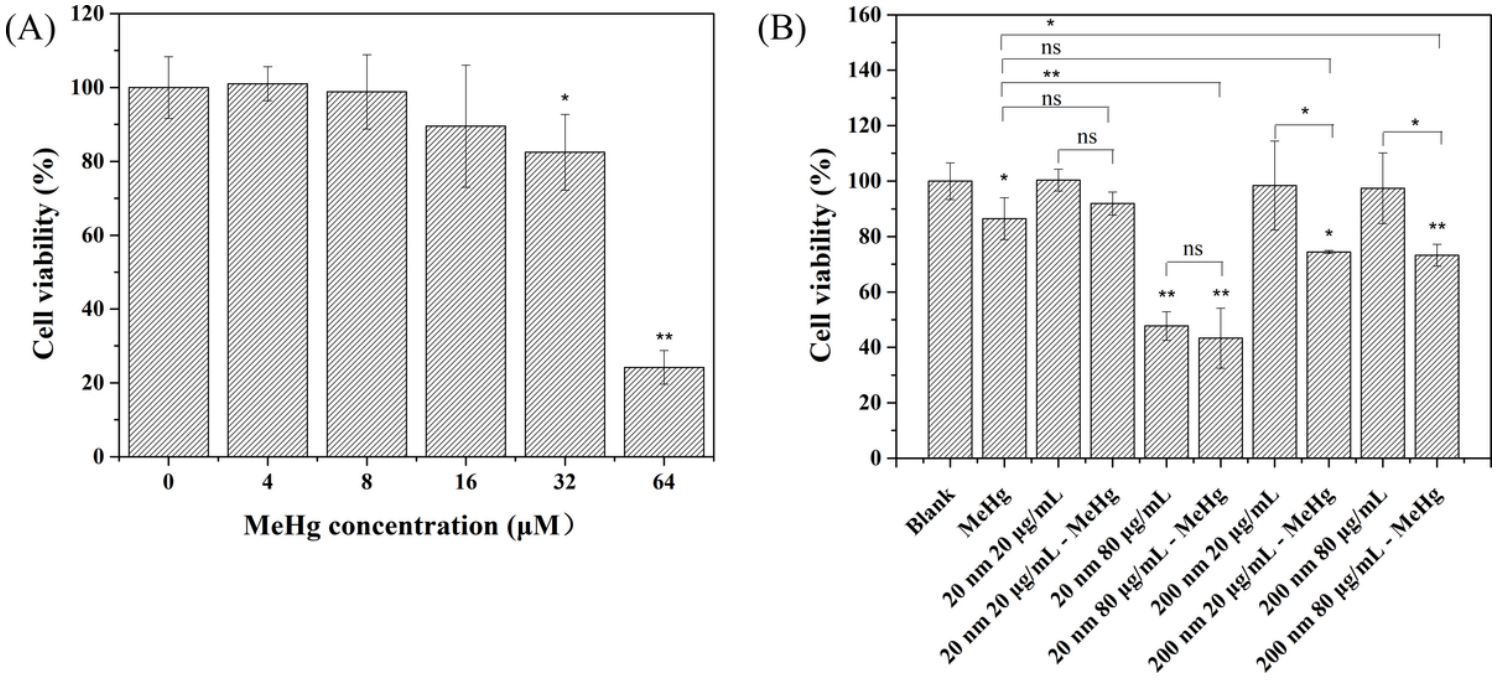

Figure 11

Effect of MeHg and PS-MeHg on the viability of Caco-2 cells. The decreasing effect of different concentrations of (A) MeHg and (B) PS-MeHg on cell viability. (*$p < 0.05$, **$p < 0.01$)

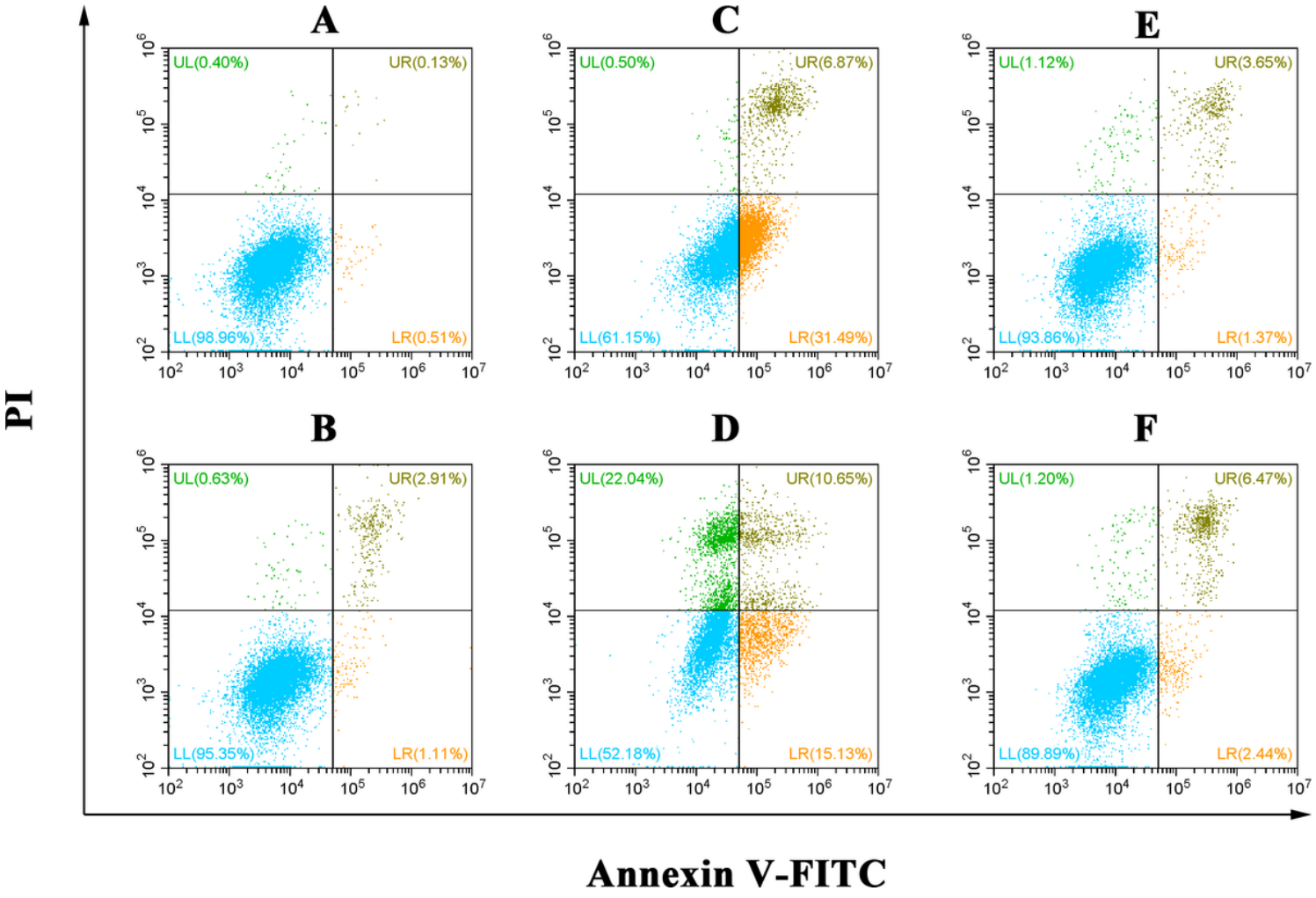

Figure 12

Effect of PS+MeHg on apoptosis of Caco-2 cells. (A) Control group. (B) 32 μM of MeHg. (C) 20 μg/mL of PS200-MeHg. (D) 80 μg/mL of PS20-MeHg. (E) 20 μg/mL of PS200-MeHg. (F) 80 μg/mL of PS200-MeHg.

Supplementary Files

This is a list of supplementary files associated with this preprint. Click to download.

- Additionalfile1.docx
- Additionalfile2.docx
- FigureS1.tif
- FigureS2.tif
- FigureS3.tif
- Graphicalabstract.tif